SPACE WEATHER, VOL. 11, 394–406, doi:10.1002/swe.20064, 2013

The 10.7 cm solar radio flux ($F_{10.7}$)

K. F. Tapping[1]

Received 26 March 2013; revised 7 June 2013; accepted 10 June 2013; published 12 July 2013.

[1] The 10.7 cm solar radio flux, or $F_{10.7}$ is, along with sunspot number, one of the most widely used indices of solar activity. This paper describes the equipment and procedures used to make the measurements and to calibrate them, and discusses some of the "most-asked" questions about the data.

Citation: Tapping, K. F. (2013), The 10.7 cm solar radio flux ($F_{10.7}$), *Space Weather*, *11*, 394–406, doi:10.1002/swe.20064.

1. Introduction

[2] The 10.7 cm solar radio flux ($F_{10.7}$) is one of the most widely used indices of solar activity. Its applications include use as a simple activity level indicator, as a proxy for other solar emissions or quantities which are more difficult to obtain, and also as a commonly available datum for antenna calibration. This article is an attempt to provide a comprehensive background to this index.

[3] Each value of $F_{10.7}$ is a measurement of the total emission at a wavelength of 10.7 cm from all sources present on the solar disk, made over a 1 h period centered on the epoch given for the value. This quantity is in fact a *flux density* not a *flux*, although it has become conventionally referred to as a *flux*. It has become clear that wavelengths in the region of 10 cm are best for monitoring the level of solar activity because solar emissions at these wavelengths are very sensitive to conditions in the upper chromosphere and at the base of the corona. However, the choice of a wavelength of 10.7 cm was entirely serendipitous. The roots of the program (now known as the Solar Radio Monitoring Program), and the choice of wavelength lie in the history of radar development during the Second World War.

[4] Solar radio emissions at centimeter wavelengths were first reported by *Southworth* [1945], although a number of fortuitous detections during World War II were made by users of centimetric radar systems. For example, radar operators noticed "sun strobes" (increased receiver noise levels) on their plan position indicator displays when the antenna scanned across the azimuth of the rising or setting Sun. The dissemination of this information was at the time strongly restricted, so detailed reports did not become widely available until some time after the cessation of hostilities.

[5] In Canada, as in many other countries, the wide availability of new expertise and suitable equipment led to an explosion of interest in radio astronomy. Arthur Covington and his colleagues at the National Research Council in Ottawa, who had spent the war years in radar development, used components from now surplus radar systems to make Canada's first radio telescope. The first observations were made in 1946. The designed operating wavelength of the radar components used was 10.7 cm (a frequency of 2.8 GHz), which set the operating wavelength of the radio telescope. Due to the limited sensitivity of the instrument, only solar emissions could be detected. When a series of calibrated measurements were made over many days, two things emerged: the measured flux measurements corresponded to disk brightness temperatures much larger than 6000 K (the temperature of the photosphere), and equally surprisingly, the solar flux densities at this wavelength varied from day to day. The connection between sunspots and solar centimetric emissions was discovered independently by *Covington* [1947, 1948], *Lehaney and Yabsley* [1949], and through a statistical study, *Denisse* [1948]. *Covington* [1947] used the edge of the Moon during a solar eclipse to identify a significant emission contribution associated with a large active region. The utility of what became known as $F_{10.7}$ as an indicator of the level of solar activity led to the continuation of measurement to the present day and to the program becoming a data service.

[6] Consistent Canadian measurements of $F_{10.7}$ began in 1947, with the measurements being made at a site to the south of Ottawa, Ontario. However, urban encroachment and implementation of increasingly high-powered radars at Ottawa International Airport produced a worsening interference environment, and in 1962, a new facility was built at the Algonquin Radio Observatory, located in a provincial park some 250 km west of Ottawa. The Ottawa facility was then closed. A second flux monitor was installed at the Dominion Radio Astrophysical Observatory, near Penticton, British Columbia, to provide an additional 3 h of observations each day. In 1979, Arthur Covington retired, and in 1983, when the last members of his original group retired, a new group was formed, with the mandate to review and upgrade all aspects of

[1]Dominion Radio Astrophysical Observatory, National Research Council, Penticton, British Columbia, Canada.

Corresponding author: K. F. Tapping, Dominion Radio Astrophysical Observatory, National Research Council, PO Box 248, Penticton, BC, V2A 6J9, Canada. (ken.tapping@nrc-cnrc.gc.ca)

1542-7390/13/10.1002/swe.20064

the program. In 1990, following the closure of the Algonquin Radio Observatory, the program, together with its upgraded instruments, were relocated to the Dominion Radio Astrophysical Observatory. The original Dominion Radio Astrophysical Observatory (DRAO) instrument was shut down. The program remains at that location to the present day.

[7] The early measurements of solar centimetric emissions were made using relatively small antennas, having beams subtending solid angles larger than that subtended by the solar disk, so no determinations of the distribution of emission could be made on any routine basis. These spatially integrated emissions were categorized on the basis of their characteristic timescale of variation into three identifiable components: a rapidly varying or *R* component, comprising emissions varying over timescales in the second-minute range, perhaps as long as an hour. Slower variations were lumped into a slowly varying or *S* component. Extrapolation to zero activity suggested an underlying constant, base level, which became called the quiet sun, or *Q* component. The terms *R* and *Q* have fallen out of use, and these components are now known, respectively, as bursts and the quiet sun background emission. The slowly varying component originates primarily in active regions; its intensity is a measure of the overall level of solar magnetic activity and has a broad spectral peak at about 10 cm wavelength. The $F_{10.7}$ values comprise contributions from the *S* component and the quiet sun background, and sometimes from radio bursts.

[8] The new solar radio group (formed in 1983) had fewer staff resources than the original group, so one unfortunate change was an unavoidable reduction in the level of manual data processing in the routine daily operation of the program, especially taking into account the level of training required and the need for long-term data consistency. Continued operation would require a much higher level of automation. For the long-term utility of any extended time series of data, critical issues are availability, absolute calibration accuracy, data consistency, and statistical homogeneity. These are highly dependent on the hardware used and its evolution, data analysis methods, and upgrade policies. In this paper, we will discuss the 10.7 cm solar radio flux monitoring program with particular attention to these issues.

2. What is $F_{10.7}$?

[9] A 10.7 cm solar flux measurement is a determination of the strength of solar radio emission in a 100 MHz-wide band centered on 2800 MHz (a wavelength of 10.7 cm), averaged over an hour. It is expressed in *solar flux units* (*sfu*), where 1 sfu = 10^{-22} W m^{-2} Hz^{-1}. It comprises a time-varying mix of up to three principal emission mechanisms which may be differently distributed over the solar disk and may vary independently with time. It contains thermal free-free emission from the chromosphere and corona, and from concentrations of plasma supported in the chromosphere and corona by active region magnetic fields. Over sunspots, where the magnetic fields are sufficiently strong for the electron gyrofrequency to exceed about a third of the observing frequency, thermal gyroresonance greatly increases the optical thickness of the radiating medium, producing bright, compact sources. In addition, nonthermal emissions might be present. Solar radio emissions are described in detail in monographs by *Kundu* [1965] and *Kruger* [1979]. Earlier discussions of $F_{10.7}$ are given by *Tapping* [1987], *Tapping and DeTracey* [1990], and *Tapping and Charrois* [1994].

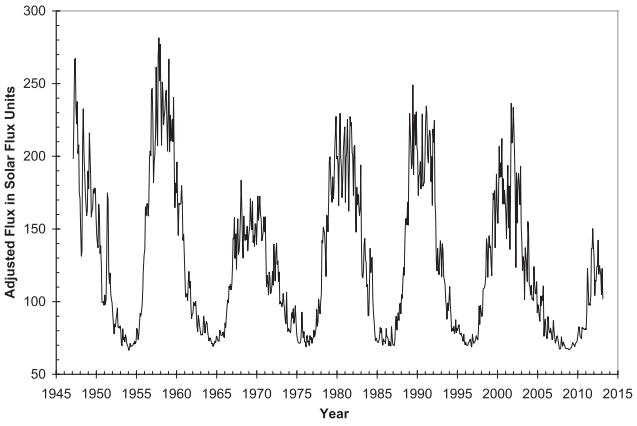

Figure 1. Monthly averages of the adjusted (scaled for an Earth-Sun distance of 1 AU) $F_{10.7}$ values since 1947.

[10] Figure 1 shows a plot of monthly-mean values of $F_{10.7}$ from the beginning of systematic observations in 1947 to March 2013. The values have been adjusted to correct for the annually changing distance between the Earth and Sun. The 10–13 year solar activity cycle is very obvious. The large variations around the maxima are due to the appearance and decay of active regions. Individual solar activity cycles vary from one to another in peak value, shape, and duration. Note that there is some activity even around solar minima. Since there is always some level of magnetic activity, it is not clear that the value of $F_{10.7}$ ever truly reflects a totally inactive Sun, even during the extended and deep minimum between cycles 23 and 24. It is also not clear what constitutes a truly "Quiet Sun" at that wavelength.

[11] The total emission from the solar disk at centimeter wavelengths may vary in intensity over a wide range of timescales, ranging from fractions of a second to years. Transient emissions from flares often show variations over milliseconds. Most bursts also vary in intensity on minute timescales. Changes over hours may be related to the evolution of active region structures or the decay of nonthermal emission from accelerated electrons produced by flares and trapped in loops. The evolution of active regions can cause variations over days to a month or so. *Gaizauskas et al.* [1983] showed that active regions form and decay within *complexes of activity*, which may persist for several months. Finally, the global ebb and flow of activity over

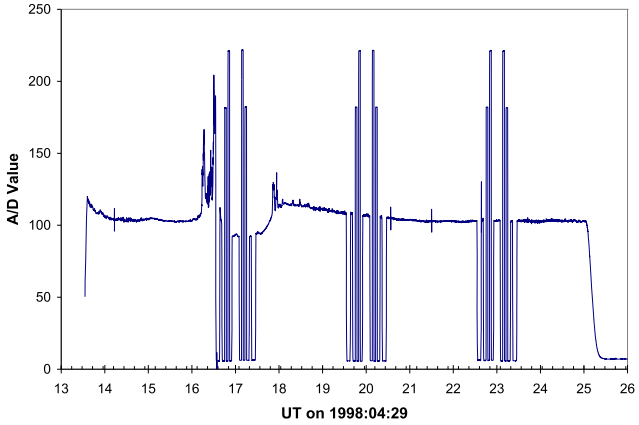

Figure 2. The continuous record file for 29 April 1998.

the solar cycle has a timescale of years. This wide range of timescales suggests that, depending upon the level and nature of activity, $F_{10.7}$ suffers from a varying degree of undersampling.

[12] In the early years of the program, attempts were made to remove bursts and other rapidly varying emissions from the flux determinations. This was done manually by staff who were very familiar with the data and observing procedures. Some flare-related emissions are easy to identify; others are not. While elevated emissions due to residual nonthermal electrons may be appropriate for excision, a period of heating and cooling in an active region is a valid contribution to the *S* component and to the flux value. Moreover, these contributions may be very difficult to distinguish.

[13] This data filtering procedure has been discontinued for two reasons: one was the staffing issue mentioned earlier. Second, many applications require the measured flux value, not a value that has been modified. Subsequently, practice has been to distribute the data as measured and to provide auxiliary data so that users could apply whatever data modification procedures they require. These are the *Continuous Record Files*, which are recordings of the flux monitor outputs with a sampling rate of 1 sample/s, taken for as long as the Sun is above the horizon each day, which show the context of the three flux determinations. An example of a day's Continuous Record (or CR) file is shown in Figure 2, which shows the file for 29 April 1998. On the left, the increase in level as the Sun rises is seen. The decrease thereafter is the reduction of thermal emission from the ground as the Sun gets higher above the horizon. The three clusters of level changes during the day are the three flux determinations. The fall in level at sunset is evident. Since the transition to the next UT day occurs while observations are being made, it is convenient to let the time advance above 24 and to reset the clock during the night. A small flare occurred during the day which disrupted one flux determination. The level was still elevated during the next.

3. Flux Monitors

[14] The flux measurements are made using two small radio telescopes, referred to as flux monitors, running in parallel, with one acting as a hot backup for the other. Each comprises a 1.8 m diameter paraboloid on an equatorial mount connected via a waveguide run to the receiver system. The two flux monitors and the solar building are shown in Figure 3. The instrument in the foreground, to the south of the building containing the receivers and computers, is Flux Monitor 1 (FM1), and the one in the background, north of the building (mounted on the tower), is Flux Monitor 2 (FM2). The default instrument is normally Flux Monitor 2. FM2 is mounted to the north of the building because when it is looking over the building, the Sun is at its highest elevation.

[15] Both flux monitors have identical receiver systems. The basic arrangement is shown in Figure 4. Each receiver system comprises two receivers, designated "A" and "B." When these receivers were built, analog/digital converters having more than 12 bits were expensive, so to get the required dynamic range, each receiver has two outputs, each with its own analog/digital converter channel: a "High-Sensitivity Channel" and a "Low-Sensitivity Channel." The former is about 100 times more sensitive than the latter. The receivers are very simple, each consisting of a string of three 2800 MHz amplifiers connected through filters. The combination of a large dynamic range and linearity required renders the usual methods for gain stabilization impractical, making more "brute force" methods appropriate. Gain instabilities arise generally through power-supply drift, unwanted feedback, or temperature variations, so we tried hard to minimize these.

[16] Fortunately, for solar observations, extremely low noise temperatures are not needed, so the receiver

Figure 3. The flux monitors. Flux Monitor 1, the secondary instrument is in the foreground; Flux Monitor 2, the primary instrument is in the background, on the tower.

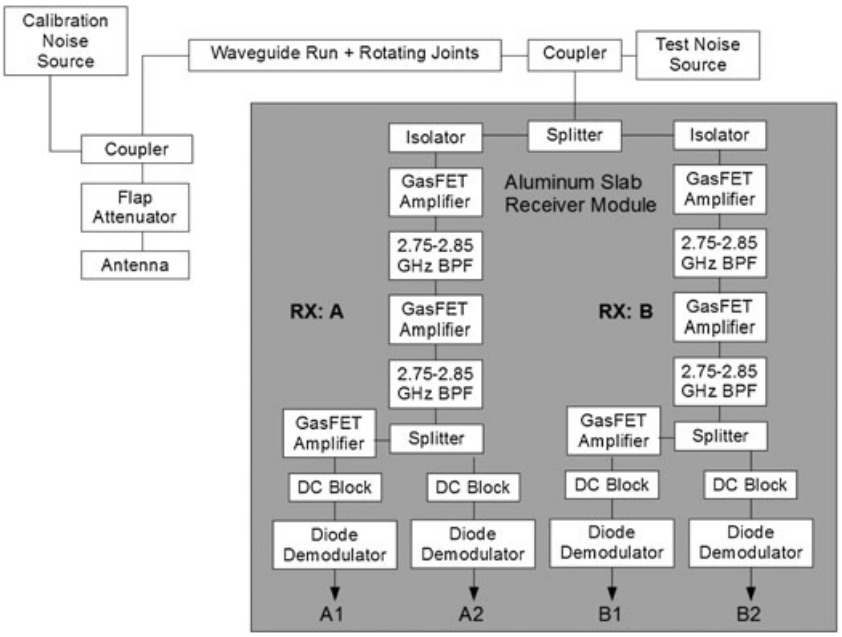

Figure 4. Block diagram of the receiver system in the flux monitors. The primary and secondary instruments are identical.

components need not be distributed between the focus of the antenna and the solar building. All the radio frequency components other than the calibration and system check noise sources are embedded in machined slots and holes in an aluminum slab 60 cm square and about 8 cm thick. They are therefore screwed to a very large heat sink with a long thermal time constant (which is increased by surrounding the slab with a draft screen). The building is air conditioned. Mounting the cables in slots and the other components in custom-machined holes, covered with a snugly fitting lid, greatly reduces unwanted feedback. Even a tiny bit of positive feedback can seriously degrade the system stability. The receiver components and postdemodulation components have their own power supplies with no common grounds. A block diagram of the receiver system used in both flux monitors is shown in Figure 4. The shaded area in the diagram represents the slab heat sink. The other (postdemodulation) components are mounted on aluminum slab heat sinks 1.5 cm thick.

[17] The signals are brought from the antenna to the receiver by means of a waveguide run (WR284). This incorporates two rotating joints (one for hour angle and the other for declination), a 1 m section of flexible waveguide to accommodate antenna tilt adjustments, and a 10 m run of sealed, copper waveguide into the solar building. A calibration noise signal of known value is injected into the waveguide as close as possible to the antenna feed. Temperature regulation of this noise source was found impractical within the space available, so it is mounted in a heat sink surrounded by insulation, with a temperature sensor fixed to the heat sink, close to the noise source. The calibration value is compensated for deviations of noise source temperature from the temperature at which it is calibrated.

[18] A second noise source, designated the system check noise source, is located in the solar building, at the bottom end of the waveguide run. A small amount of noise is injected into the waveguide as needed. The exact value of the amount of power injected need not be precisely known, but that value needs to remain constant. The noise source is attached to a heat sink and located within the draft screen, and together with the receivers, in the temperature-regulated building. The ratio of the signal levels from the calibration and system check noise sources provide an indication of health of the waveguide run and rotating joints. This diagnostic tool once led to our locating a small break in the flexible waveguide. The flux values showed no evidence of being affected by this small problem. However, eventually, water ingress or wasps taking up residence could have caused the problem to become serious.

[19] The dual-output configuration makes it possible to adequately measure flux values while being able to accommodate fairly large bursts. Figure 5 shows an example of a strong burst recorded by the high- and low-sensitivity channels of the A receiver on FM2. The high-sensitivity channel (blue), which is used for flux measurements and recording small bursts, overloaded cleanly at 1300 solar flux units, but the peak flux density was easily recorded by the low-sensitivity channel (red). The correspondence between the two channels below the overload level is excellent, but at low flux levels, the resolution limit of the low-sensitivity channel is obvious.

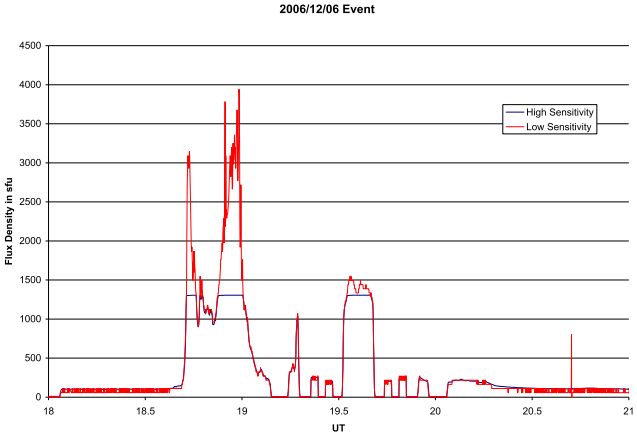

Figure 5. A burst observed on the high- and low-sensitivity channels of Receiver A of FM#1 on 6 December 2006. Note that since that time, the choreography of the flux measurement has changed to that described here.

4. Measuring $F_{10.7}$

4.1. The Flux Determination Method

[20] When the flux monitor antenna is pointed at the Sun, the output voltage from the receiver system is given by (assuming square law demodulation):

$$V_{\text{sun}} = k\Gamma\zeta\left(T_{\text{sun}} + T_{\text{sky}}(\phi,\theta) + T_{\text{ground}}(\phi,\theta) + T_{rx}\right) + V*, \quad (1)$$

where k is the Boltzmann's constant, Γ is the gain-bandwidth product of the receiver system, and ζ is the constant of proportionality between the voltage output from the demodulator and the power into it. T_{sun} is the power from the Sun arriving at the antenna, and T_{ground} and T_{sky} are, respectively, the powers received from the sky and from the ground surrounding the flux monitor antenna. $V*$ is the offset bias voltage applied to the analog/digital converters to best use their dynamic range, plus whatever other stray offset voltages that inevitably arise in the system. The ground and sky temperatures are functions of the direction in which the antenna is pointed (ϕ is the antenna azimuth and θ the elevation). The quantities in the equation pertaining to the flux monitor are assumed to be constant or to vary only slowly with time. None of them is assumed to be known a priori.

[21] In conventional radio astronomy, the contribution made to the receiver output by the source being measured is isolated by moving the antenna far enough off-source for that contribution to the receiver output to vanish. In general, the antennas used in radio astronomy have beam widths in the region of arc min, so the antenna may be needed to be moved off source by less than a degree, in which case, all the other contributions can usually be assumed constant, so the difference between the on- and off-source measurements is proportional to the flux density of the source. However, this assumption is questionable when applied to the antennas used to measure solar flux values. To see the whole solar disk with uniform sensitivity, as required to produce an unbiased flux value, the antenna beam width needs to be in the region of 3°–5°. To make an off-source measurement, the antenna will have to be moved several degrees or more. It is doubtful that the ground radiation and possibly other contributions would remain constant over such a large antenna movement. Until the middle 1980s, the measurement method involved going off-source to the zenith and the use of measured values for the ground radiation. This need for external parameters specific to the instrument and site makes the flux determination process sensitive to changes in the immediate surroundings, such as the growth of trees. To avoid these problems, a new method which is not as environment-sensitive was subsequently implemented. This method is described here, and illustrated in Figure 6.

[22] The segment of sky covered by the 1 h period during which the flux determination is made is divided into four arcs. As the Sun moves from arc to arc, the antenna is moved to track through the arcs so that by the end of the flux determination, measurements have been made for each arc with the Sun present and without it. The choreography shown in the figure is listed below.

[23] 1. When the Sun enters, A_1 data logging begins, building the on-source average S_1, which is completed when that arc is exited.

[24] 2. The antenna is then moved to the beginning of A_3, which is far enough from the Sun for it to be considered "off-source," and tracked through this arc, accumulating the off-source average O_3.

[25] 3. By the time the antenna reaches the end of A_3, the Sun is reaching the beginning of A_2. The antenna is pointed back at the Sun and tracks through A_2, accumulating the on-source average S_2.

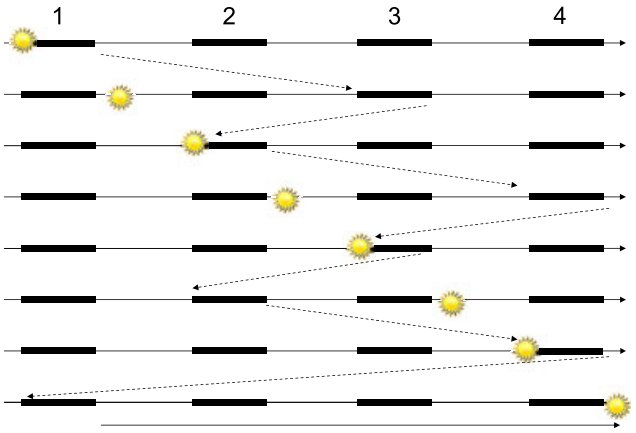

Figure 6. The flux determination procedure. Each of the stacked horizontal lines depicts the segment of the solar track containing four arcs. Time increases downward. The set of arcs spans about 15°.

[26] 4. On completion of this observation, the antenna is moved off-source to the beginning of A_4. It tracks through this arc, accumulating the off-source average O_4.

[27] 5. By this time, the Sun is reaching the beginning of A_3, and the antenna tracks it through this arc, accumulating the on-source average S_3.

[28] 6. The antenna then moves off-source to the beginning of arc A_2, tracks through it, and accumulates the off-source average O_2.

[29] 7. By this time, the Sun is reaching the beginning of A_4, and the antenna tracks it through this arc, accumulating the on-source average S_4.

[30] 8. The antenna then moves off-source to the beginning of arc A_1, tracks through it, and accumulates the off-source average O_1.

[31] In the formula below, the values are all averages over their particular arc. Ground and sky noise contributions will vary from arc to arc because the antenna is moving.

[32] When the Sun is present, we obtain the following average:

$$S_i = k\Gamma\zeta\left(T_{\text{sun}} + T_{rx} + T_{\text{ground},i} + T_{\text{sky},i}\right) + V*, \tag{2}$$

where i is the arc number ($1 \leq i \leq 4$). When the Sun is absent,

$$O_i = k\Gamma\zeta\left(T_{rx} + T_{\text{ground},i} + T_{\text{sky},i}\right) + V*. \tag{3}$$

[33] In the middle of each observation, at the center of the track through each arc, a calibration noise source is turned on for a minute. This is done for the on-source and off-source blocks. The on-source values are used for linearity checks and are not further discussed here. When the calibration noise source is switched on and the antenna is off-source, we get:

$$C_i = k\Gamma\zeta\left(T_{\text{cal}} + T_{rx} + T_{\text{ground},i} + T_{\text{sky},i}\right) + V*. \tag{4}$$

[34] The value of the calibration signal, T_{cal}, is obtained through bench measurements. The size of the change in receiver output due to the calibration noise source provides a monitor of gain stability through the flux measurement process.

$$\Delta S_i = S_i - O_i = k\Gamma\zeta T_{\text{sun}} \tag{5}$$

and

$$\Delta C_i = C_i - O_i = k\Gamma\zeta T_{\text{cal}}; \tag{6}$$

therefore,

$$T_{\text{sun},i} = T_{\text{cal}} \times \frac{\Delta S_i}{\Delta C_i}. \tag{7}$$

[35] The flux value in solar flux units is related to T_{sun} by

$$F_{10.7} = (2 \times 10^{22})\frac{kT_{\text{sun}}}{A_{\text{eff}}}, \tag{8}$$

where A_{eff} is the effective collecting area of the antenna. The effective collecting area of a dish antenna is difficult to establish, so we use a separate, calibration antenna (see next section). The output from this calibration process is four estimates of $F_{10.7}$. The plot of the chart record file shown in Figure 7 shows the three daily flux determinations and pointing checks.

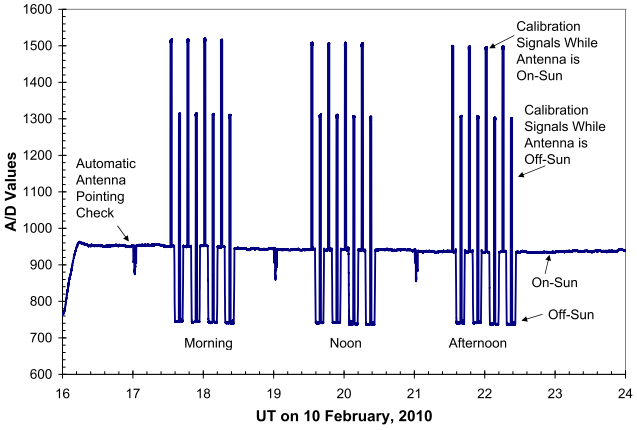

Figure 7. A continuous record file from flux monitor 2 on 10 February 2010, showing the three daily flux determinations.

4.2. The Observed, Adjusted, and International Union for Radio Science (URSI)-Series D Flux Values

4.2.1. The Observed Flux

[36] The Observed Flux are the values that would be incident on the top of the atmosphere or at ground level in the absence of that atmosphere. Tropospheric attenuation at 10.7 cm wavelength is significant, about 5% when the Sun is at an elevation of 10°, falling to roughly 1% when the Sun's elevation is 30°. Fortunately, this attenuation is mainly due to molecular oxygen, the concentration of which does not vary significantly with time. We endeavor to correct for this, to produce an estimate of the flux value that is incident on the top of the atmosphere. Since the solar flux is not measured for small angles of elevation (less than about 10°), a simple "slab" model for the troposphere is adequate. This formula yields a correction factor by which the measurement is multiplied. It is the one used by Covington et al. since the early days of the program:

$$\text{atmloss} = (0.9875) + (0.0115) \times \csc(\text{elevation}). \tag{9}$$

[37] The Observed Flux is the measured value multiplied by atmloss.

[38] These flux values are intended for use for terrestrial applications such as estimating upper atmospheric heating, forecasting ionospheric communication quality, and antenna calibration.

4.2.2. The Adjusted Flux

[39] Since the Earth's orbit around the Sun is elliptical, the Observed Flux values are modulated by the changing Earth-Sun distance. When the flux values are being used as an index of solar activity, perhaps being compared with other activity indices, such as sunspot number, the modulation is undesirable and can be corrected by multiplying by the current Earth-Sun distance in astronomical units squared (1 AU is the average distance between the Earth and Sun), which makes the flux values refer to a

constant distance of 1 AU. These flux values are called the *Adjusted Flux*. Since the computers controlling the flux monitors have ephemeris programs built in, the Adjusted Flux is computed at the time of the measurement.

4.2.3. The URSI Series-D Flux Value

[40] In the early days of solar radio monitoring, absolute measurements of the solar flux density were made at many wavelengths, using many different radio telescopes and a variety of different measurement methods. Reconciling these measurements with one another and integrating them into a calibrated spectrum of solar radio emission became an important issue for discussion at URSI (the International Union for Radio Science). By fitting spectra to collections of data and then looking at the discrepancies between the measurements and the fit, it became possible to estimate some calibration correction factors for the various observatories. This calibration work is discussed by *Tanaka* [1969] and in more detail and incorporating additional data by *Tanaka et al.* [1973]. The value allocated to the 10.7 cm (Ottawa) flux values was 0.9. To apply this adjustment, the adjusted flux values would be multiplied by this 0.9 factor. This correction was not applied to the observed or adjusted flux values as measured, but as a new column in the reports, new value, termed the *URSI Series-D Flux*, which is 0.9 × Adjusted Flux.

5. Flux Calibration

[41] The flux monitor measurements are calibrated using a noise level that is injected via a directional coupler into the signal line as close as possible to the antenna feed horn. The exact value of the injected noise level depends upon the noise power produced by the noise source and the coupling factor of the directional coupler. In principle, these can be measured on the bench or with more difficulty on the antenna. The latter approach better takes into account the effects of local mismatches and other inevitable imponderables. However, the result of this process is a measurement of the antenna temperature increase due to the Sun (T_{sun}). This is related to the flux density by the relationship

$$F_{10.7} = (2 \times 10^{22}) \frac{2kT_{\text{sun}}}{A_{\text{eff}}}. \quad (10)$$

[42] The effective collecting area of the antenna (A_{eff}), which is a fraction, is typically around 50%–60% of the physical area. It is a function of the feed horn properties, its precise position with respect to the focus of the dish, the surface accuracy of the dish, and how much of its area is shadowed by the feed horn, its supports, and the signal waveguide. It is very difficult to determine. The easiest solution is to calibrate the flux monitor against a reference calibration antenna, which in this case is a pyramidal horn. The effective collecting area of these antennas can be determined from first principles.

Figure 8. Calibration Horn system seen from the East. Two identical horns are mounted piggyback. The electronics is housed in the casing on the back of the horns. Antenna driving is manual, using the large declination scale for pointing. The upper horn is the one currently used.

5.1. The Calibration Standard Horn

[43] A gently tapering, pyramidal horn antenna has the great advantage that its effective collecting area can be calculated from its dimensions and the observing wavelength alone. When our horn system was originally implemented, the effective collecting area was calculated using the method of *Schelkunoff and Friis* [1952]. The application in this instance is described in detail by *Steen* [1967]. Since that time there has been some refinement of horn gain calibration methods, but to maintain consistency of the data, especially with duplicate databases scattered around the world, we continue to use the referenced method. The relevant dimensions are: aperture: 1.22 m × 0.91 m, length from phase center to center of aperture plane: 2.44 m, and the calculated gain with the polarization in the plane of the shorter aperture dimension is 428 (26.3 dB) at 10.7 cm wavelength, which corresponds to an effective collecting area of 0.39 m^2, and an aperture efficiency of about 35%. Although measurements should be made with no blockage in front of the horn apertures, we found that to keep out birds and wasps, we had to install open-weave fabric over the apertures. This does not detectably affect measurements made when the fabric is completely dry. This is not a major issue in the arid Okanagan climate, at least during the summer and autumn. The antenna is fixed so that it points south, with its elevation being adjustable. Observations are made by allowing the Sun to drift through the antenna beam. The horn calibration system is shown in Figure 8. The standard antenna used for calibrating the $F_{10.7}$ data consists of two identical horns mounted piggyback as a meridian transit instrument. This provides the opportunity to make comparative measurements between them. In principle, it would be

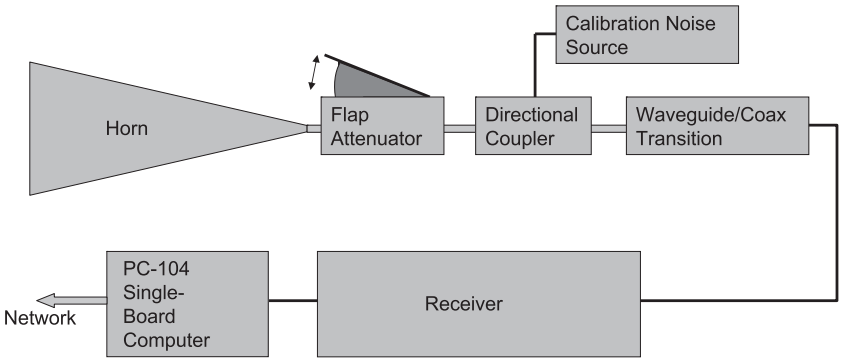

Figure 9. Block diagram showing the layout and main components of the horn calibration system. The thick, grey line indicates waveguide connections; thinner, black lines indicate wires or cables.

more convenient to implement flux monitors with horn antennas. However, they are much more unwieldy to mount and require more careful attention when being used to make measurements.

5.2. The Receiver

[44] The horn receiver system comprises two units: a calibrator, which is connected directly to the output from the horn, and a receiver module. The two units are located in a housing attached to the horn structure and connected by rigid, copper-clad coaxial cable. The calibrator module consists of a flap attenuator, (which when inserted into the waveguide effectively terminates it with an ambient-temperature matched load,) a calibration noise source, and a directional coupler for injecting a known quantity of noise into the signal line. All these components are in WR284 waveguide and waveguide/coaxial transformer to launch the signal into the coaxial cable that takes it to the receiver. The receiver module is identical to one channel of a flux monitor receiver, a single-board computer is incorporated for data logging. Both units can be removed either independently or as a unit for bench calibration or maintenance. A block diagram of the calibration horn system is shown in Figure 9

5.3. Horn Flux Measurements

[45] The observation consists of a drift transit recording of the Sun with regular injections of calibration noise. These noise levels need to be known in order to establish the antenna temperature increase due to the Sun. The calibration noise level is determined in two ways. The primary method is to remove the receiver system from the horn antenna and do bench measurements, where liquid nitrogen cold loads can be conveniently employed. An auxiliary method, which makes it possible to reduce the frequency with which the facility has to be dismantled for bench tests, is to point the horn antenna at the zenith and use the sky as the cold load, while continuing to use the flap attenuator as the hot load. Measurements in two observing sessions separated by a year indicated an antenna temperature when pointed at the zenith of 9–11 K. This agrees with earlier measurements made by Covington.

[46] Horn measurements are set up manually, and a computer logging system is used to record the receiver output. Initially, the horn antenna is pointed at the zenith, and a series of measurements are made of the sky noise, with the flap attenuator inserted, and with the calibration noise source switched on. This is used as a check of the calibration value. The antenna is then set to the elevation of the Sun at transit.

[47] Measurements are started about 2 h before transit and ended 2 h after. The antenna azimuth is fixed due south, and over the 4 h, the Sun drifts through the antenna beam. A typical horn observation is shown in Figure 10.

[48] Processing a drift transit observation using the horn antenna involves a number of important considerations.

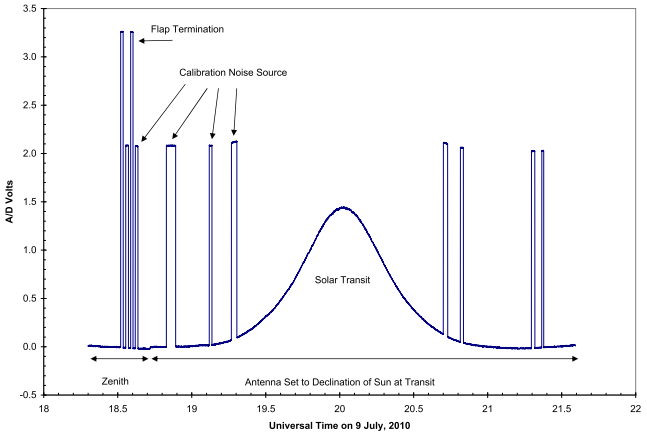

Figure 10. A transit observation of the Sun made using the calibration horn. Around 18:30 UT, the antenna was pointed to the zenith, and the calibration value was checked using the flap attenuator/termination. A small rise in level can be seen as the antenna moved down to the elevation of the Sun at transit. The noise source was turned on manually several times during the transit.

First, the observation takes a long time, over 3 h. Since the receiver is mounted on the horn antenna, where on occasion the temperature varies considerably, the gain of the receiver may also drift during the observation. This variation is monitored through frequent injections of noise from the calibration noise source.

[49] The observation in Figure 10 shows a number of things that need to be dealt with. The baseline slope is almost certainly due to gain drift, but since the baseline values include an unknown offset voltage, they cannot be simply scaled to correct for gain variations. A line is fitted to the data and subtracted from the observational values to remove the baseline slope. There are two reasons for this: to de-skew the transit profile to facilitate the profile fitting process discussed below, and to provide an estimate of the baseline value under the peak of the transit, designated B_0. Any variation in the gain is indicated by changes in the sizes of the level changes when the calibration noise source is turned on and off multiple times during the observation. A line is fitted and the record scaled accordingly. The level change that would occur if the calibration noise source were turned on at the precise moment of transit is estimated by interpolation (C_0). Finally, a polynomial is fitted to the top half of the transit in order to use more of the data to estimate the peak value (S_0). The antenna temperature increase due to the Sun, and the solar flux density is then:

$$T_{\text{sun}} = \left(\frac{S_0 - B_0}{C_0 - B_0} \right) T_{\text{cal}}, \tag{11}$$

so

$$F = (2 \times 10^{22}) \frac{2k}{A_{\text{eff}}} T_{\text{sun}}, \tag{12}$$

where T_{cal} is the calibration noise level in Kelvins.

[50] A calibration session comprises transit observations repeated over several or more days, compared with cotemporal measurements of the solar flux made using the flux monitors. The horn measurement is used to set the calibration flux value in the flux monitors (F_c), to make their measurements agree with the horn measurements. In practice, the difference has only once been more than one solar flux unit. When differences are not larger than one sfu, the calibration of the flux monitors is left unchanged. Inevitably, due to the differences between the measurement techniques, the impact of a burst on the flux monitor and horn measurements will differ, so observations bearing bursts or other short-term variations are not used.

[51] Horn calibration checks are laborious and can only be made during the summer months. A rough check of calibration and equipment integrity can be made by comparing the flux determinations made by the two flux monitors, since these are more or less identical and fully independent systems. The quantity (FM1 − FM2)/(FM1 + FM2) gives a useful indication of the deviation if any between the two instruments. Figure 11 is a plot of this quantity (multiplied by 100) for part of 2012.

[52] One interesting issue that arose resulted from using aluminum for the receiver housing on the horns.

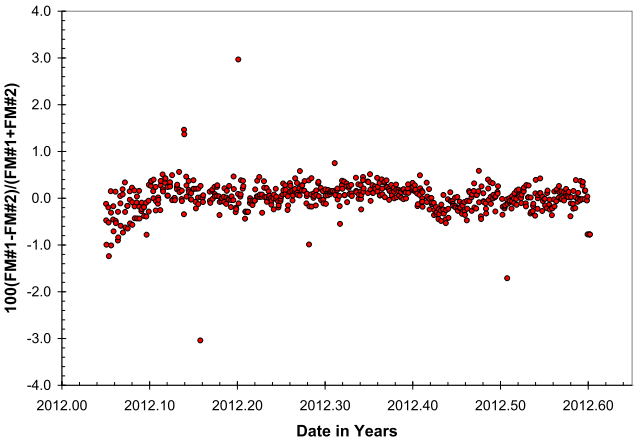

Figure 11. The deviations between the two flux monitors during 2012.

Even though aluminum is highly reflective in the optical part of the spectrum, it is highly absorbent in the infrared. The result was that the housing became extremely hot during the observations, overpowering the cooling fans. This is the main cause of the gain (baseline) drift in the plot in Figure 10. The horns themselves are made of galvanized steel, a material that does not have this problem. Aluminium housings need to be painted with white, infrared-scattering paint.

6. Overall Data Accuracy

[53] The distribution of the ratio between the flux measurements shown in Figure 12 suggests a standard deviation of about 0.5%. If this is equally distributed between the two flux monitors, where their outputs vary independently, the standard deviation of the fluctuations in one of the flux monitors would be about 0.4%. Due to the nature of the horn measurements, it is difficult to establish a distribution for random measurement errors. However, considering the hardware similarity, it is reasonable to assume the measurements to be similarly distributed, in which case, the standard deviation of the ratio between the horn measurements and cotemporal flux measurements would also be in the region of 0.5%. In this case, most of the flux monitor measurements should be within 1% of the horn measurement. The calibration process usually involves comparative observations over several or more days, so the error should be significantly less than this.

[54] At the beginning of each horn measurement, the antenna is pointed at the zenith and measurements made of the change in receiver output when a matched load of known temperature was connected and when the calibration noise source in the receiver was switched on. This provides a check of the noise source value:

$$\frac{T_{\text{cal}} - T_{\text{zenith}}}{T_{\text{load}} - T_{\text{zenith}}} = \frac{x_{\text{cal}} - x_{\text{zenith}}}{x_{\text{load}} - x_{\text{zenith}}} = Y, \tag{13}$$

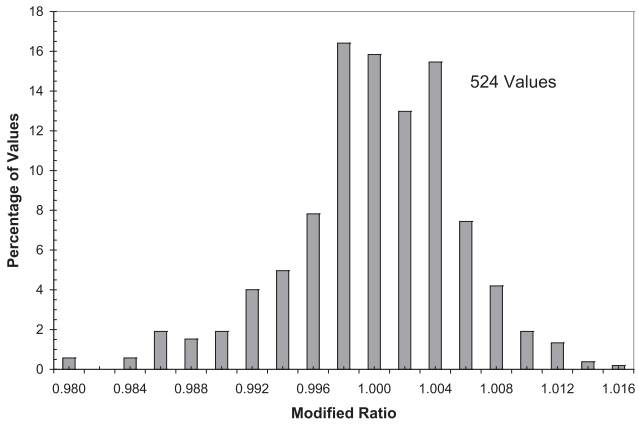

Figure 12. The distribution of the ratio measurements after detrending.

so

$$T_{cal} = Y(T_{load} - T_{zenith}) + T_{zenith}. \quad (14)$$

[55] A digital thermometer sensor connected to the load indicates its temperature to within 0.1 K. The greatest uncertainty is in the estimation of the antenna temperature of the horn when pointed at the zenith. A series of measurements made at DRAO suggest a zenith antenna temperature in the range 9–11 K. A zenith antenna temperature of 10 K is assumed. This translates to an error window in estimating the noise source value of about 1%, which probably comprises a combination of systematic and random contributions. Crudely combining these errors gives a result of about 1.4%, which taking into account averaging of several measurements and assuming an equal mix of systematic and random contributions, we take as an error range of 1%.

[56] In the above discussion, it is implicitly assumed that all the errors are multiplicatively applied to the solar flux value. When the Sun is quiet, the fluxes are smaller, and the additive noise contributions and errors become more important. Although we have not fully quantified these, we have incorporated this error contribution into our conclusion about the (usual) standard of flux accuracy. *The $F_{10.7}$ values are deemed to be accurate to one solar flux unit or 1% of the flux value, whichever is the larger.*

7. Other Flux Issues

[57] Having one observing site making three spot measurements between sunrise and sunset raises important issues pertaining to the utility of the data. The main ones are discussed below.

7.1. Undersampling

[58] Three flux determinations are made each day, at 1700, 2000, and 2300 UT, except during the winter months, where the low elevation of the Sun (DRAO lies at +50° latitude) and the hilly terrain, forces the times to be changed to 1800, 2000, and 2200 UT. Each flux determination takes 1 h and takes no account of the solar radio emissions recorded outside the intervals covered by the measurements. Since the active region emissions contributing to the slowly varying emission (and $F_{10.7}$) may vary over hours or less, there may be a significant degree of undersampling. In addition, there could be a contribution by a burst. The undersampling means there is a possible error if one uses a flux value in an application involving a different time from that at which the flux measurement is made.

[59] It is impossible to make a definitive statement about the relationship between a spot measurement at noon and the value of the solar flux averaged over the day. During the summer of 1993 an experiment was carried out by *Tapping and Charrois* [1994] to learn a little more about this issue. The horizon elevation was measured using a theodolite at the antenna location, and the ground radiation as a function of azimuth and antenna elevation modeled. The terrain was extremely dry and there was no rain over the period, so the modeled ground radiation could be assumed constant with time and only a function of antenna direction. The estimated ground and atmospheric loss were subtracted from the receiver output, and the remainder, which was assumed of solar origin, was averaged over the day. At the time (during the declining phase of cycle 22), we found that on 95% of the days, the noon measurement was within two solar flux units of the value averaged from sunrise to sunset.

7.2. Errors Due to the Measurement Process

[60] Although a determination of $F_{10.7}$ takes an hour, the resulting number is not simply an average value over that hour. During that hour, there are four blocks where the antenna is on-source, together with the same number of off-source blocks and periods where the antenna is in motion. Between 30% and 40% of the hour is actually spent making valid solar observations. Therefore, on fortunately rare occasions, when the solar emission is varying, even making an observation or measurement over the same time interval as that used for measuring $F_{10.7}$ need not produce the same value.

7.3. Use as a Proxy

[61] Deriving a proxy involves plotting the quantity against $F_{10.7}$ and fitting a curve that is subsequently used to estimate the desired quantity from $F_{10.7}$ data. If the modeled parameter varies slowly, it is best to apply a low-pass filter to the $F_{10.7}$ data before making the comparison and in its subsequent application. If there are possible sampling issues with the parameter to be proxied, it might be appropriate to apply a low-pass filter identically to the parameter being proxied and to $F_{10.7}$, which is severe enough to reduce both quantities to statistical similarity.

7.4. Data Consistency and Continuity

[62] Consistency and continuity of the time series are critical requirements for the $F_{10.7}$ data. Data consistency is best maintained by frequent calibration against a reliable standard. Continuity can be improved by running two

independent but identical systems in parallel. Then, if the designated primary flux monitor fails, a backup instrument is running in the background, producing data that can be distributed instead. The availability of a backup makes maintenance and equipment improvements much easier. Calibration against the horn antenna system is time-consuming and can only be done in the dry, summer months. In the shorter term, we use the ratio of the measurements made simultaneously by Flux Monitors 1 and 2 as a rough check of calibration stability and equipment operation. Figure 12 shows the ratio of the flux measurements made with Flux Monitors 1 and 2 for the first half of 2012.

[63] The longer-term fluctuations in the values are removed by subtraction of a sixth-order fitted polynomial. The distribution of the short-term fluctuations preferentially selected by this subtraction process is shown in Figure 12.

8. A Note on Antenna Calibration

[64] The $F_{10.7}$ values are often used for the calibration of networks of antennas operating at 10.7 cm wavelength (weather radar networks, for example). However, when doing this, there are some important provisos to consider.

[65] The solar flux value is an equally weighted summation of the emission at 10.7 cm wavelength from all sources present on the disk, including thermal emission from the disk. To achieve this equal weighting, the antenna beam-shape must not taper by more than a percent or so between the edge of the solar disk and the center and must have the antenna boresight directed at the disk center, not the centroid of the radio emission (which could be different if there is a bright active region close to the solar limb). If such a bright active region is present, simply pointing the antenna boresight in the direction of the emission maximum could produce a different measurement. Moreover, if the antenna being calibrated has a narrow beam, where the sensitivity varies significantly over the 0.25° angular radius of the solar disk when the antenna boresight is directed at the disk center, the calibration will be in error by an amount that can be estimated if the Sun is quiet, and the only emission is that from the disk, but by an amount difficult to estimate if activity centers are present. There is no reliable way that measurements at 10.7 cm wavelength can be applied to solar calibrations of antennas operating at other wavelengths. This is due to the 10.7 cm solar radio flux comprising a time-varying mix of emission mechanisms, each with its own unique spectrum, that together produce a spectrum that varies with time in a manner that cannot be usefully estimated on the basis of measurements made at a single frequency.

9. Summary and Discussion

[66] This article is an attempt to provide in one place a discussion of the 10.7 cm solar radio flux and to include answers to some of the most often asked questions regarding it and its applications. The underlying science is discussed only to the degree necessary. It has some advantages over sunspot number, the only index with a longer record, but also has shortcomings that need to be taken into account. Its major advantage is that it can be an objective measurement made in (more or less) the same way, using the same or similar equipment for an indefinite duration. Its long-term stability can be maintained by comparison with an absolute calibration standard.

[67] The section comprises four parts. First, there is a summary covering the main points about $F_{10.7}$; second, there is a discussion of some current science using this index and underlining the continuing need for continuous, consistent time series of solar index data covering as long a period of time as possible; third, discussion of new developments that are either in progress or desirable; and finally, some comments on the importance of ground-based solar monitoring programs.

9.1. Summary

[68] Three flux determinations are made each day. They take an hour and are centered on the stated epoch of the measurements, which in the summer are 1700, 2000, and 2300 UT each day, and due to the latitude, hilly horizon and the low elevation of the Sun, 1800, 2000, and 2200 UT in the winter. Each measurement takes an hour. The integrated solar radio emission at 10.7 cm can vary over short periods; bursts can vary dramatically over seconds or less, and active region emissions due to evolutionary processes can vary over timescales as short at an hour or so. The more rapid variations tend to occur around solar activity maxima, at which times, three measurements a day with none taken during the night may lead to significant undersampling. To some extent, the context of the measurements, and therefore the effects of undersampling, can be obtained from the *Continuous Record Files*, which are files of the receiver outputs recorded at 1 sample/s from sunrise to sunset.

[69] Over the hour taken for each flux determination, four measurements are made, along with off-source observations. Taking into account off-source blocks and the time taken by the antenna moving on- and off-source, only about a third of the time during the hour is actually spent observing the Sun. If the solar radio emissions are varying over hour timescales, a measurement of the solar radio flux made in a different way could result in a different value, which is, however, equally valid. For this reason, drift scans made using the calibration horn are not used for system calibration checks if there is evidence of rapid variability. In cases of use of the flux values for antenna calibration, it is highly unlikely that the same measurement method will be used, and at the same time, so serious measurements should not be attempted at times the solar radio emissions are rapidly varying.

[70] Two other issues that often arise in applications of the flux data in antenna calibrations are the beam widths of the antennas being calibrated and how they are being calibrated, and utility of the flux data for calibrations at other wavelengths. If the beam width of the antenna being

calibrated is small enough for the gain to taper by more than 1% or so over a quarter of a degree (the angular radius of the solar disk), it cannot easily be calibrated using $F_{10.7}$ data because the antenna being calibrated will weight the contributions from different points on the solar disk in its own unique way. In addition, if there are bright sources located toward the edge of the solar disk, the error introduced by the weighting will be larger, and if the antenna is pointed by maximizing the received signal power, the antenna may not be pointed at the disk center, introducing additional errors. With respect to using $F_{10.7}$ to estimate fluxes at other wavelengths, as required for some antenna calibration applications, solar radio emissions at centimeter wavelengths comprise a time-varying mixture of emission mechanisms, each having its own particular time-varying spectrum. There is therefore no reliable way in which a single-wavelength measurement, such as $F_{10.7}$ can be used to estimate the flux density at another wavelength with any dependable accuracy.

9.2. $F_{10.7}$ as a Diagnostic of Solar Behavior

[71] Historical data of various quality, data back thousands of years in some cases, show the Sun's behavior has on occasion changed significantly. However, not all changes are clearly identifiable through examination of single indices. Since the various solar activity indices currently measured quantify different phenomena in the Sun, they are stethoscopes on different aspects of solar activity, and comparisons between them can be used as sensitive detectors of changes in solar behavior. For example, soon after the peak of cycle 23, a change in the relationship between $F_{10.7}$ and sunspot number values occurred, and which continues into cycle 24 [*Tapping and Valdes*, 2011]. Similarly, $F_{10.7}$ is playing in an important role in the current controversy regarding the current decline the darkness of sunspots. Reduction in the contrast of sunspots against the surrounding (brighter) photosphere suggests a weakening of the sunspot magnetic fields and consequently less inhibition of convective heat flow from below [*Svalgaard and Hudson*, 2010; *Livingston et al.*, 2012; *Penn and Livingston*, 2006; *Hill et al.*, 2011; *Dikpati et al.*, 2010].

9.3. Augmenting the Program

[72] Since the beginning of systematic $F_{10.7}$ measurements in 1947, the range of applications has changed and expanded, and user needs in many areas have become more rigorous. Some of these involved improvements in accuracy, data availability, and clarification of the basic properties of the measurements. However, although is a need to maintain the current data time series over coming decades, there are ways the program can be usefully augmented. Three main areas for this augmentation are: (a) mitigating the problem of undersampling, (b) implementing multiwavelength measurements to common standards, and (c) integration of radio imaging into solar monitoring.

9.3.1. Undersampling

[73] To some extent, the having only three precise flux determinations each day can be mitigated by recording the solar emissions over the day, so in a given day, the data comprises a record of solar emission intensity upon which three precise flux determinations are superimposed. However, at any given location, over a year, there will be a large amount of time the Sun is below the horizon. For a ground-based monitoring system, a reasonable solution is to have multiple stations scattered in longitude around the world, so that well before the Sun has got too low at any given station for useful observations to be made, at another station, located further west, the Sun is high enough for useful observations to be made. With enough overlap, a continuous 24 h/d record can be built up. Ideally, the stations should be close enough for adjacent stations to have a flux determination in common. In that way, an increased fault tolerance is obtained, and a single system calibration facility such as the horn antenna system can be daisy-chained around the world. To ensure data homogeneity, similar flux determination methods should be used.

9.3.2. Multiwavelength Flux Measurements

[74] $F_{10.7}$ is a composite, comprising contributions from two or more emission mechanisms. Over active regions, where plasma concentrations are supported in magnetic fields where the electron gyrofrequency is small (less than a quarter?) compared with the observing frequency, the emission is predominantly thermal, free-free emission. Over sunspots, where the magnetic fields are strong enough for the electron gyrofrequency to exceed about a third of the observing frequency, thermal gyroresonance becomes important. Electrons are accelerated in active regions, particularly during transient events such as flares. These can interact with the magnetic fields to produce gyrosynchrotron emission. Beams of accelerated electrons can interact with the plasma to produce a variety of plasma waves. However, these processes are generally more important at decimeter and longer wavelengths. Since all these contributions may vary with time, largely independently, there is no way the spectrum can be usefully estimated on the basis of a measurement made at a single wavelength. Multiwavelength observations are needed, and these measurements need to be made with high precision, at the same time and in the same manner, so that they can be assembled into a meaningful spectrum.

[75] Apart from various applications involving single wavelengths, such as the calibration of antennas, there are needs for measurements where the contributions by the various emission mechanisms have been separated. For example, some applications use $F_{10.7}$ as a proxy for extreme ultraviolet and ultraviolet irradiances, which are used for things such as ionospheric modeling and estimation of upper-atmospheric heating. A shortcoming of $F_{10.7}$ in its current form is that it comprises contributions from free-free emission from plasma concentrations over plage (which coincides roughly with bright EUV/UV emission), and from gyroresonance over sunspots (which

are darker at EUV/EUV wavelengths). Therefore, reliable removal of the gyroresonance contribution could, if consistent enough, yield a better proxy for EUV/UV emissions. To address this and other issues, "Next Generation Solar Flux Monitor (NGSFM)" is being built. It will operate with the existing flux monitors but is not intended to replace them. It will measure fluxes at 1.4, 1,6, 2.8, 4.9, 8.3, and 10.6 GHz, and a spectrometer will simultaneously monitor the entire frequency range from 1.4 to 10.6 GHz. Using a progressively under-illuminated paraboloid, all measurements will be made in the same manner, at the same time, and using almost identical hardware.

[76] Another improvement implemented in the Next Generation Solar Flux Monitor (NGSFM) is the multiple calibration noise levels. Three noise sources can be switched on in various combinations to give seven different calibration levels. This arrangement was chosen to avoid the use of mechanically switched devices, which can fail and eventually develop unpredictable losses.

9.3.3. The Role of Solar Radio Imaging

[77] Single-antenna solar flux monitors are inexpensive to construct, operate, and upgrade; they are also relatively easy to calibrate. These are all very important points when implementing programs intended to be continued indefinitely. Imaging at 10.7 cm (and other wavelengths) would make it possible to identify the sources of the radio flux with particular magnetic structures and better separate emission mechanisms. In addition, with the current changes in solar behavior, the relationships between the radio emissions and their host magnetic structures would provide a useful diagnostic tool. Daily images would be excellent, but regular images taken less often would be extremely useful. A suitable solar imager would adequately sample (as closely as possible) all angular scales in the image with high time resolution. The Expanded Very Large Array certainly offers the required capabilities but is unlikely to be available for routine, patrol observations. Mapping the disk emission and the multiple sources contributing to $F_{10.7}$ [e.g., *Schmahl and Kundu*, 1995] would provide better understanding of the relative influences of sunspots, coronal plasma, and disk emission in the future.

9.4. Final Comment

[78] In an age of space-borne solar observations, there is still a place for ground-based solar monitoring at radio wavelengths, such as 10.7 cm. The measurements date back to 1947, and the low maintenance, improvement, and operational costs it should possible to keep these programs going indefinitely. Instruments can be duplicated, maintained, and upgraded easily, and data gaps avoided. Additional radio data, such as multiwavelength observations and radio images of the solar disk, will add context and weight to the flux measurements rather than replace them. Moreover, today, with the vulnerability of essential infrastructure higher than ever, the need for reliable, ongoing stethoscopes on the Sun as the engine driving space weather, is higher than ever.

[79] **Acknowledgments.** The longevity, continuity, and consistency of the $F_{10.7}$ record is due to the contributions of many, including J. Bastien, M. Bell, C. Bergeron, N. Broten, A. Covington, P. Gagnon, W. Medd, J. Moore, C. Philipson, E. Sheehan, M. Steen, E. Stevens, and R. Stuart. I also thank the referees for their detailed and thoughtful suggestions. The 10.7 cm solar radio flux data are provided by the National Research Council of Canada, with the participation on Natural Resources Canada and support by the Canadian Space Agency.

References

Covington, A. E. (1947), Microwave solar noise observations during the eclipse of November 23, 1946, *Nature*, *159*, 405–406.

Covington, A. E. (1948), Solar noise observations on 10.7 cm, *Proc. IRE*, *36*, 454–457.

Denisse, J.-F. (1948), Etude des émissions radioélectriques solaires d'origine purement thermique, PhD thesis, Univ. de Paris, Paris.

Dikpati, M., P. A. Gilman, G. de Toma, and R. K. Ulrich (2010), Impact of changes in the Sun's conveyor belt on recent solar cycles, *Geophys. Res. Lett.*, *37*, doi:10.1029/2010GL044143.

Gaizauskas, V., K. L. Harvey, J. W. Harvey, and C. Zwaan (1983), Large-scale patterns in solar activity during the ascending phase of cycle 21, *Astrophys. J.*, *65*, 1056–1065.

Hill, F., R. Howe, R. Komm, J. Christensen-Dalsgaard, T. P. Larson, J. Schou, and M. J Thompson (2011), Large-scale zonal flows during the solar minimum – Where is cycle 25?, *Bull. Am. Astron. Soc.*, *43* (16.10.).

Kruger, A. (1979), Introduction to solar radio astronomy and radio physics, *Geophys. and Astrophys. Monogr., vol. 16*, D. Reidel, Dordrecht, Netherlands.

Kundu, M. R. (1965), *Solar Radio Astronomy*, John Wiley, New York.

Lehaney, F. J., and D. E. Yabsley (1949), Solar radiation at 1200 Mc/s, 600 Mc/s and 200 Mc/s, *Aust. J. Sci. Res. Ser. A*, *2*, 48–62.

Livingston, W., M. J. Penn, and L. Svalgaard (2012), Decreasing sunspot magnetic fields explain unique 10.7 cm radio flux, *Astrophys. J. Lett.*, *757*, 8.

Penn, M. J., and W. Livingston (2006), Temporal changes in sunspot umbral magnetic fields and temperatures, *Astrophys. J.*, *649*, L45–48.

Schelkunoff, S. A., and H. T. Friis (1952), *Antennas - Theory and Practice*, 528–529, John Wiley, New York.

Schmahl, E., and M. R. Kundu (1995), Microwave proxies for sunspot blocking and total irradiance, *J. Geophys. Res.*, *100*, 19,851–19,864.

Southworth, G. C. (1945), Microwave radiation from the Sun, *J. Franklin Inst.*, *239*, 285–297.

Steen, M. M. (1967), Gain calculations of a 2800 MHz standard horn for solar noise observations?, *Rep. ERB-758*, Natl. Res. Counc. of Can., Ottawa, Ontario. Canada.

Svalgaard, L., and H. S. Hudson (2010), The solar microwave flux and sunspot number, in *SOHO-23: Understanding a Peculiar Solar Minimum*, *ASP Conf. Ser.*, *428*, edited by S. R. Cranmer, J. T. Hoeksema, and J. L. Kohl, pp. 325–328, Astronomical Society of the Pacific, San Francisco, Calif.

Tanaka, H. (1969), The absolute calibration of variable flux density in the microwave region, *Prog. Radio Sci.*, *2*, 1966–1969.

Tanaka, H., J. P. Castelli, A. E Covington, A. Kruger, T. L. Landecker, and A. Tlamicha (1973), Absolute calibration of solar flux density in the microwave region, *Sol. Phys.*, *29*, 243–262.

Tapping, K. F. (1987), Recent solar radio astronomy at centimeter wavelengths: The variability of the 10.7 cm flux, *J. Geophys. Res.*, *92*, 829–838.

Tapping, K. F., and D. P. Charrois (1994), Limits to the accuracy of the 10.7 cm flux, *Sol. Phys.*, *150*, 305–315.

Tapping, K. F., and B. DeTracey (1990), The origin of the 10.7 cm solar flux, *Sol. Phys.*, *127*, 321–332.

Tapping, K. F., and J. J. Valdes (2011), Did the Sun change its behaviour during the decline of cycle 23 and into cycle 24?, *Sol. Phys.*, *272*, 337–350.